Nuclear pore disassembly from endoplasmic reticulum membranes promotes Ca^{2+} signalling competency

Michael J. Boulware and Jonathan S. Marchant

Department of Pharmacology, University of Minnesota Medical School, Minneapolis, MN 55455, USA

The functionality of the endoplasmic reticulum (ER) as a Ca^{2+} storage organelle is supported by families of Ca^{2+} pumps, buffers and channels that regulate Ca^{2+} fluxes between the ER lumen and cytosol. Although many studies have identified heterogeneities in Ca^{2+} fluxes throughout the ER, the question of how differential functionality of Ca^{2+} channels is regulated within proximal regions of the same organelle is unresolved. Here, we studied the *in vivo* dynamics of an ER subdomain known as annulate lamellae (AL), a cytoplasmic nucleoporin-containing organelle widely used *in vitro* to study the mechanics of nuclear envelope breakdown. We show that nuclear pore complexes (NPCs) within AL suppress local Ca^{2+} signalling activity, an inhibitory influence relieved by heterogeneous dissociation of nucleoporins to yield NPC-denuded ER domains competent at Ca^{2+} signalling. Consequently, we propose a novel generalized role for AL – reversible attenuation of resident protein activity – such that regulated AL (dis)assembly via a kinase/phosphatase cycle allows cells to support rapid gain/loss-of-function transitions in cellular physiology.

(Received 29 February 2008; accepted after revision 25 April 2008; first published online 1 May 2008)
Corresponding author J. S. Marchant: Department of Pharmacology, University of Minnesota Medical School, 6–120 Jackson Hall, 321 Church St SE, Minneapolis, MN 55455, USA. Email: march029@umn.edu

The endoplasmic reticulum (ER) is an intracellular Ca^{2+} storage organelle that integrates mechanisms for Ca^{2+} uptake and release in response to cellular stimulation (Meldolesi & Pozzan, 1998; Baumann & Walz, 2001; Blaustein & Golovina, 2001; Papp *et al.* 2003). Functioning as a synthetic factory, scrapyard and synchronized distribution network, the ER tailors regional infrastructure and asset localization to support diverse subcellular functions using its sizeable membrane surface area (∼50% total membrane surface) and luminal volume (∼10% of cellular volume; Voeltz *et al.* 2002) to anchor reactions that support, as well as terminate, cellular viability.

To support such specialization, the ER is highly plastic in morphology and function (Meldolesi & Pozzan, 1998; Baumann & Walz, 2001; Blaustein & Golovina, 2001; Voeltz *et al.* 2002; Papp *et al.* 2003; Borgese *et al.* 2006). Globally, the ER acts as a pervasive network through which ions, proteins and exogenous labels rapidly equilibrate (Terasaki & Jaffe, 1991; Mogami *et al.* 1997). Such global interconnectivity ensures that ER proteins are able to interact with ER-resident partners whose trans-domains lie within the nucleoplasm or cytoplasm, as well as signalling complexes that sense mitochondrial, extracellular and transcellular environments, underscoring the role of the ER as a key information-relaying superhighway. Despite such interconnectivity, many discrete ER subdomains exist beyond the classic divisions of rough ER, smooth ER and the two nuclear envelope (NE) membranes. These encompass transitional, peroxisomal, junctional and nucleoplasmic ER, the diads, triads and peripheral couplings of sarcoplasmic reticulum, as well as a variety of ER specializations in cells as diverse as oocytes and plant growth tips. In addition, there exist functional heterogeneities in ER Ca^{2+} uptake, release and buffering that have, as yet, no clear structural basis (Lievremont *et al.* 1994; Rooney & Meldolesi, 1996; Golovina & Blaustein, 1997). A final complexity is that compartmentalization of ER Ca^{2+} signals results not only from static heterogeneities in the distribution of Ca^{2+}-handling proteins but also from more ephemeral assemblies of Ca^{2+}-release channels, Ca^{2+} pumps and Ca^{2+}-binding proteins that alter their localization in response to cell stimulation (Wilson *et al.* 1998; Liou *et al.* 2005; Roos *et al.* 2005; Tateishi *et al.* 2005; Chalmers *et al.* 2006). Collectively, all these data suggest that the ER is composed of a collection of rapidly differentiable subdomains with discrete Ca^{2+}-handling properties.

Mechanistic insight into the biogenesis of ER subdomains, and how residency of ER proteins within these specializations affects their functionality, are important considerations in understanding first, how

This paper has online supplemental material.

 DOI: 10.1113/jphysiol.2008.153379

cells regulate their overall responsiveness and second, the targeting, amplification and vectorality of cytoplasmic Ca^{2+} signals. Therefore, in this manuscript we investigated the cell biology of a discrete ER subdomain, known as annulate lamellae (AL). Numbers of these enigmatic ER structures are elevated in virally infected cells and tumours, as well as oocytes and embryos (Kessel, 1992). Previously viewed as a subdomain of the rER that warehouses excess nuclear pore complexes (NPCs), they have been extensively studied *in vitro* (Meier *et al.* 1995; Miller & Forbes, 2000) as a biochemical model for reconstituting the events of NPC assembly and nuclear envelope/germinal vesicle breakdown (NE/GV-BD). Less is known about their *in vivo* role, despite the observation that in human eggs, formation of AL is a vital postfertilization process, with AL misassembly resulting in early developmental failure (Sutovsky *et al.* 1998).

We have recently shown that during oocyte maturation, AL contribute to the biogenesis of cortical ER patches and thereby Ca^{2+} signalling competency in the mature, fertilizable egg (Boulware & Marchant, 2005). AL deliver an IP_3R complement from the ER subcortex into the peripheral shell of cortical ER that supports propagation of the fertilization Ca^{2+} wave. This transfer of the AL-derived IP_3Rs is associated with increased IP_3R overall responsiveness: whereas IP_3Rs within AL in the oocyte have a low propensity to be involved in local Ca^{2+} signalling, AL-derived IP_3Rs within cortical ER patches of the egg act as foci for Ca^{2+} wave initiation. Succinctly, these two types of ER specialization containing IP_3Rs (AL and cortical ER patches) display divergent local Ca^{2+} signalling activities. As a paradigm for how Ca^{2+} channel activity can be locally regulated between proximal areas of the same organelle, we resolved to investigate potential *in vivo* mechanisms underpinning changes in IP_3R responsiveness relative to AL dynamics throughout the time course of oocyte maturation.

Methods

Materials

Reagents were sourced as follows: Ca^{2+} indicators, caged IP_3, Alexa Fluor 488-WGA (Alexa Fluor 488 conjugated with wheat germ agglutinin), Alexa Fluor 647-WGA, tetramethylrhodamine- and Alexa Fluor-conjugated dextrans (10 kDa, 70 kDa), and jasplakinolide from Invitrogen (Carlsbad, CA, USA); D-*myo*-inositol 1,4,5-trisphosphate (IP_3) and nocodazole from EMD Biosciences (La Jolla, CA, USA); DsRed2-ER from BD Biosciences (Palo Alto, CA, USA); anti-IP_3R (sc-28613) from Santa Cruz Biotechnology (Santa Cruz, CA, USA); mab-414 (Covance MMS-120R) and anti-phosphovimentin (KAM-CC249) from Stressgen (Victoria, BC, Canada); cytochalasin B, cytochalasin D, progesterone, human chorionic gonadotropin (hCG) and okadaic acid from Sigma-Aldrich (St Louis, MO, USA); Complete protease inhibitors from Roche Diagnostics (Indianapolis, IN, USA). Nup153 conjugated with green fluorescent protein (Nup153-GFP) and GFP-vimentin were generous gifts from Drs Jan Ellenberg (European Molecular Biology Laboratory (EMBL)) and Ronald Liem (Columbia University), respectively.

Handling of oocytes and eggs

Adult *Xenopus laevis* frogs (NASCO, Fort Atkinson, WI, USA) were anaesthetized by immersion in tricaine methane sulphonate (MS 222, 0.1 g l^{-1}; buffered with 0.7 g l^{-1} sodium bicarbonate) and monitored during induction and recovery from anaesthetic following protocols approved by the Institutional Animal Care and Use Committee (IACUC) at the University of Minnesota. For fractionation experiments, oocytes were obtained following exposure of surgically removed ovarian tissue to collagenase (Sigma Type I, 0.5 mg ml^{-1}) to remove follicular cells. Eggs, obtained by shedding after hCG injection, were de-jellied in 2% cysteine and rinsed in modified Barth's solution (mM: NaCl 88, KCl 1, $NaHCO_3$ 2.4, $MgSO_4$ 0.83, $Ca(NO_3)_2$ 0.33, $CaCl_2$ 0.41, Hepes 5; and 0.05 mg ml^{-1} gentamycin, pH 7.4, 18°C) before homogenization. Frogs were killed humanely at the end of experiments. For microinjection experiments, individual stage VI oocytes were isolated and defolliculated manually with watchmakers' forceps. Oocytes were maintained in modified Barth's solution with solution changes every 12 h. cDNA vectors were subsequently injected into the germinal vesicle to ensure appropriate cellular targeting. Cells that expressed DsRed2-ER in the vegetal hemisphere (after ~48 h) were injected with caged IP_3 and fluo4-based Ca^{2+} indicators ($K_d[Ca^{2+}] = 225$ nM for imaging local Ca^{2+} signals or $K_d[Ca^{2+}] = 3\ \mu$M for imaging global Ca^{2+} signals). Curve fitting (χ^2 as criterion) was performed using Origin (OriginLab Corporation) and mono- and multiexponential fits compared using the partial (sequential) *F* test. In some experiments cells were injected with fluorescent WGA (final concentration of 5–10 μg ml^{-1}), a concentration lower than that which inhibits pore transport (Finlay *et al.* 1987). Oocytes were matured *in vitro* with progesterone (1 μg ml^{-1}).

Confocal imaging

For live cell imaging experiments, we employed two distinct confocal systems built around the same inverted microscope (Olympus IX81 ×40–60 objective lenses, NA 1.35–1.42). This system (shown in Fig. 1 of the online Supplemental material), permitted the interchangeable use of video-rate confocal and flash photolysis (for Ca^{2+} imaging), as well as multicolour confocal timelapse

imaging (for morphology) in the same cell. The need for this dual approach derived from the discrete benefits of either confocal approach. The video-rate raster-scanning laser spot system (Callamaras & Parker, 1999) well suited for localizing Ca^{2+} puffs (duration of tens of milliseconds) over short periods (seconds) within restricted regions of the ER was deleterious to the observation of ER morphology over the long time course of oocyte maturation (≤ 14 h). A swept-field confocal approach (using an arc lamp-based spinning disc system to facilitate multiwavelength imaging) was preferable for timelapse confocal imaging where low light intensities and long exposure intervals sufficed, but this method was reciprocally futile for resolving local Ca^{2+} signals at acceptable illumination intensities.

For short-term Ca^{2+} imaging (seconds to minutes), we used the 'home-brew' resonant-galvanometer, laser(488 nm)-point scanning system built around the video-port of the microscope, which provided sufficient temporal resolution (15–60 Hz) and sensitivity to resolve individual Ca^{2+} puffs (Callamaras & Parker, 1999). Ca^{2+} signals were represented as pseudo-ratios (F/F_0) of fluorescence at each pixel during a response (F) relative to resting pixel fluorescence (F_0). For timelapse imaging, we preferred an arc-lamp-based spinning-disc confocal module (Olympus DSU) with electron-multiplication CCD camera (Hamamatsu, C9100-12) attached to the epifluorescence port. The arc-lamp-based approach enabled imaging of fluorophores with discrete excitation spectra (e.g. ER (red, DsRed2-ER), NPCs (far-red, Alexa Fluor 647-WGA)), while the sensitivity of the EM-CCD and wide-field imaging approach minimized exposure times that we believe minimized phototoxicity over the lengthy timeframe of these experiments (≤ 14 h per cell). Consequently, ER remodelling could be followed in multiple AL simultaneously using timelapse confocal imaging, and then individual AL from the same field selected at appropriate time points for local Ca^{2+} imaging using video-rate confocal microscopy.

Immunoblotting

The protein content of samples was quantified using a Qubit fluorimeter and Quant-it protein assay kit (Invitrogen). Equal amounts of protein from specific fractions were subjected to electrophoresis and Western blot analysis using the Invitrogen NuPage large protein analysis system. Nitrocellulose membranes were blocked with 12% (w/v) non-fat dried milk (Flavorite) and 1% (w/v) bovine serum albumin (BSA) and probed with antibodies against IP_3R and nup62 (mab-414, see Materials). Signals were visualized using appropriate secondary antibodies coupled to horseradish peroxidase using an enhanced chemiluminescence system (Pierce, Rockford, IL, USA).

Immunocytochemistry

Cells were fixed by immersion and incubation (> 2 h) in 1% formaldehyde in methanol at -20°C. Cells were warmed to room temperature and rehydrated in PBS in a stepwise fashion (5 min rinses in a 75%–50%–25% MeOH series into 100% PBS). Cells were permeabilized (0.1% Triton X-100) and blocked (4% BSA, 1 h) and then incubated (2 h) with primary antibody in BSA (2%). Cells were rinsed in PBS (1 h) and incubated in secondary antibody in BSA (2%) overnight at 4°C. Finally, cells were rinsed (1 h, PBS) and mounted on glass coverslips using mounting media (Ted Pella Inc.).

Maturation-promoting factor (MPF) protein kinase assay

Cells were snap frozen in a minimal volume of kinase assay buffer (mM: Tris 50, NaCl 500, EDTA 4, EGTA 2, β-glycerophosphate 25, sodium orthovanadate 1, 2-mecaptoethanol 50 and a Complete protease inhibitor tablet, pH 7.5). Cells were thawed, supplemented with 50 μl kinase assay buffer per oocyte and homogenized by vigorous pipetting before being spun at 10 000 *g* for 15 min. Kinase assays (absorbance at $\lambda = 490$ nm) were performed using the Mesacup Cdc2 Kinase Assay Kit (MBL International Corp., Woburn, MA, USA) according to the manufacturer's instructions using 2.5 μl of supernatant collected as described above.

Cell fractionation and $^{45}Ca^{2+}$ flux assay

Xenopus oocytes or eggs were homogenized in buffer (pH 7.25) containing 50 mM Tris-HCl, 250 mM sucrose and a Complete protease inhibitor tablet. The resulting homogenate was centrifuged at 1500 *g* for 15 min to yield a supernatant which was then centrifuged at 142 000 *g* for 35 min to yield a microsomal pellet. The pellet was resuspended in a minimal volume of the same buffer and re-homogenized using a tight-fitting ground glass homogenizer. The sample was then layered on top of a discontinuous sucrose gradient composed of three layers at 56%, 46% and 43% sucrose in 50 mM Tris-HCl pH 7.25 and spun at 237,000 g in a SW55 swinging bucket rotor for 2.5 h. Visible material was isolated at each interface, diluted into homogenization buffer and spun at 142 000 *g* for 40 min to yield the final pellets which were solubilized in 50 mM Tris-HCl, 300 mM sucrose and a Complete protease inhibitor tablet before being snap frozen in liquid nitrogen.

For $^{45}Ca^{2+}$ uptake, equal amounts of protein from each fraction were thawed and diluted into a cytoplasmic-like buffer (mM: Pipes 20, KCl 140, NaCl 20, $MgCl_2$ 2, EGTA 1 and $CaCl_2$ 0.3, supplemented with 7 mM ATP, 10 μM FCCP and 30 μCi ml^{-1} of $^{45}Ca^{2+}$ at pH 7.0) for 20 min at

room temperature (21°C). After loading, microsomes were diluted into non-supplemented cytoplasmic-like buffer containing the indicated concentration of IP_3 or 0.1% Triton X-100 for 3 min before filtering and rinsing on a GF/B filter. Residual radioactivity was estimated by liquid scintillation counting (LS6500, Beckman).

Results

Changes in vegetal hemisphere ER morphology were followed during progesterone-evoked maturation by timelapse confocal imaging (images captured every 10 min over ~10–14 h) in cells expressing a luminal ER marker (DsRed2-ER). Before the addition of progesterone, annulate lamellae (AL) were resolved as subcortical ER densities ('cigar'-shaped structures, 10–25 μm long, ~5 μm wide; Boulware & Marchant, 2005) that remained relatively immobile in the arrested oocyte (Fig. 1*Aa*; see also Movie 1 in online Supplemental material). However, AL disappear within ~4–5 h after progesterone addition (Fig. 1*Ab*), appearing to sink deeper into the cytoplasm, an event which precedes the emergence of patch-like densities in the ER cortex of the maturing cell (Fig. 1*Ac*, Supplemental Movie 2).

A simple way of visualizing the process of ER remodelling throughout maturation in a single cell, that facilitates comparison of experimental manipulations is shown in Fig. 1*B*. This figure (a 'lamellogram') is a thresholded '*xt*' ('linescan') projection of a ~14 h timelapse in a single cell that tracks ER morphology

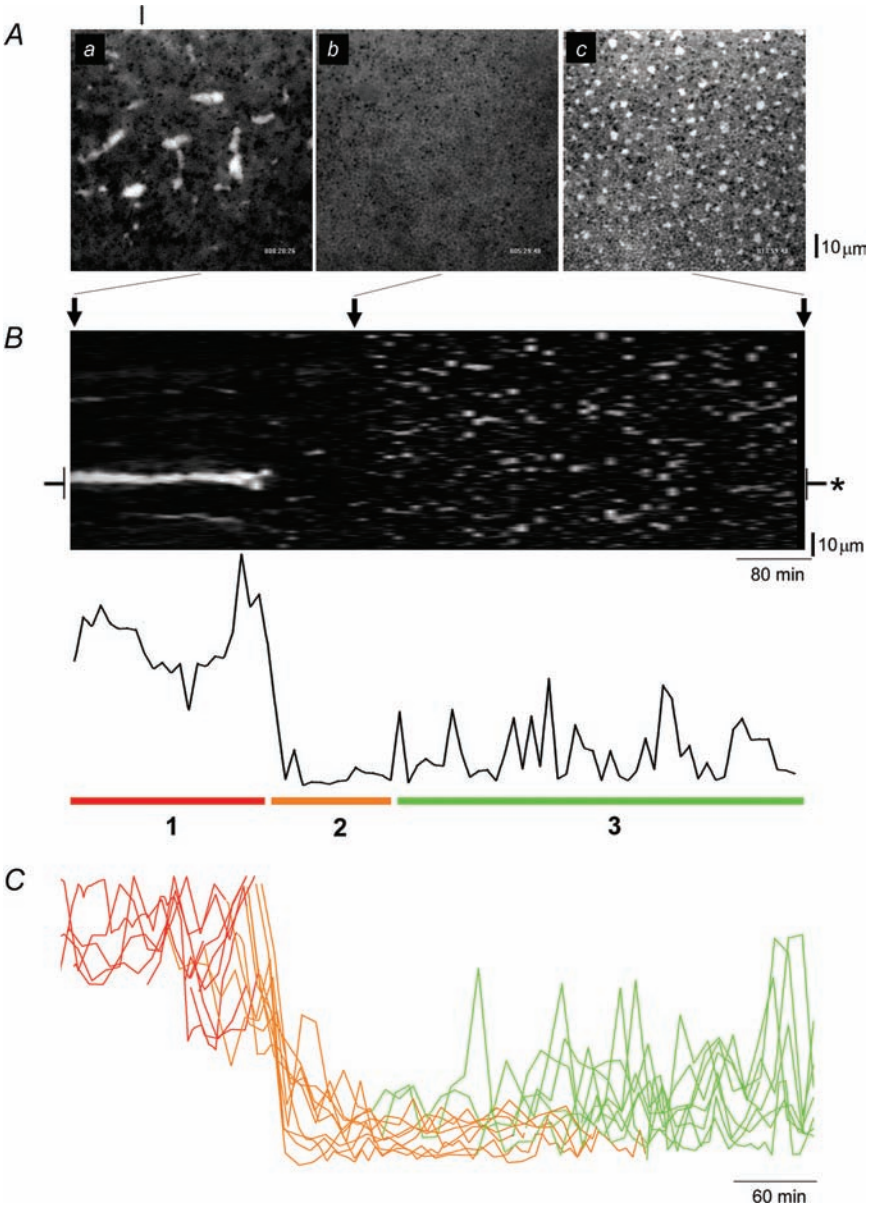

Figure 1. ER subdomain morphology during *Xenopus* oocyte maturation
A, lateral ('xy') confocal images of DsRed2-ER fluorescence in the vegetal hemisphere of the same *Xenopus* oocyte, taken ~20 min (*a*), 5.5 h (*b*) and 14 h (*c*) from a timelapse movie (Supplemental Movie 2) started on addition of progesterone (1 μg ml^{-1}). The vertical line indicates the linescan position used for the projection in *B*. *B*, upper panel, projection ('*xt*') of a timelapse stack into a single 'lamellogram' image, showing fluorescence across a single spatial dimension (vertical axis) over time (horizontal axis). Positions in this projection corresponding to the images shown in *A* are indicated by arrows; lower panel, fluorescence intensity profile measured from region (asterisked) on lamellogram. *C*, overlay of fluorescence profiles from multiple lamellograms ($n = 10$) revealing three phases of ER remodelling (1, red; 2, orange; 3, green) are conserved in different cells. Given the variable timeframe of maturation in single cells, profiles are aligned to the end of phase '1' in each timelapse record.

(vertical) over time (horizontal). Although considerable spatial information is lost, the simple plot condenses all pertinent morphological and kinetic information into a single, comprehensible plot. The lamellogram and associated fluorescence profile (Fig. 1*B*) reveal three phases of AL remodelling: (1) 'AL persistence' after progesterone addition, (2) the short, abrupt phase of 'AL disappearance', and finally (3) the phase of 'ER patch emergence', in which smaller, motile ER patches develop that frequently transect the scanline (see later). Each of these phases was observed in all maturing oocytes, although the duration of specific phases showed appreciable variability between cells (Fig. 1*C*).

To image NPC dynamics within AL during maturation, we expressed a GFP-tagged nucleoporin (Nup153-GFP, a basket nucleoporin; Stoffler *et al.* 1999) or labelled endogenous nucleoporins (including nup62, nup98 and nup214; Miller *et al.* 2000) with fluorescent wheat germ agglutinin (WGA) conjugates. Timelapse imaging of NPC dynamics using either approach (Fig. 2*A*) showed that both NPC labels were rapidly lost from AL around the time that this ER subdomain disappeared ('phase 2', Fig. 1*B*) and neither NPC label reappeared in cortical ER densities during the late phase of maturation (Supplemental Movie 3). Simultaneous dual-emission imaging of DsRed2-ER and Alexa Fluor 488-WGA (Fig. 2*A*) confirmed the differential behaviour of NPC and ER markers in the same cell over the entire maturation time course. Further, the fluorescence profiles associated with these dual wavelength projections indicated a small delay (range of 20–90 min; mean of 41 ± 28 min, $n = 5$) between the loss of NPCs and the disappearance of AL (asterisk, Fig. 2*A*). To substantiate this observation, lateral ('*xy*') confocal images, captured at shorter time intervals during this period, were analysed. These images surprisingly revealed a heterogeneous, 'patchy' dissociation of NPC label from AL, leaving a variegated ER subdomain of adjacent NPC-replete and NPC-denuded regions (Fig. 2*Ba*, Supplemental Movie 4). In higher-magnification images of individual AL, vesicle-like structures labelled with NPC markers could be seen in the vicinity of AL during this period of NPC dissociation (Fig. 2*Bb*, Supplemental Movie 5).

Do macroscopic Ca^{2+} dynamics change during this phase of ER remodelling? Previous comparison of cellular Ca^{2+} dynamics only at the extremes of the maturation process (i.e. immature oocyte *versus* fertilizable egg; Boulware & Marchant, 2005) demonstrated an increase in magnitude, initial rate of cytosolic Ca^{2+} clearance and Ca^{2+} signal duration (owing to regenerative propagation of the fertilization Ca^{2+} wave) after maturation in the vegetal hemisphere. In essence, the initial component of the decline in the oocyte Ca^{2+} transient is accelerated, while the terminal phase(s) are lengthened – adaptations that can easily be tracked via a single ratio ($t_{55} : t_{10}$; ratio of times taken for fluorescence to decay to 55% and 10% of peak value). Using a low-affinity Ca^{2+} indicator to track Ca^{2+} dynamics throughout maturation, it was observed that the period of ER remodelling correlated temporally with these transitions in the cellular Ca^{2+} transient (Fig. 2*C* and *D*). That ER remodelling occurs contemporaneously with changes in Ca^{2+} signalling should not imply a sole causative relationship – it is probably one of many factors to impact the whole-cell Ca^{2+} signature (El-Jouni *et al.* 2005) – however, we do infer from these data that the extensive AL remodelling occurs while the Ca^{2+} signal of the maturing cell is being customized to support fertilization.

Next, we attempted to image localized IP_3R activity in AL throughout maturation to resolve at what point IP_3R activity increased in these ER subdomains. In particular, the simultaneous occurrence of NPC-replete and NPC-depleted areas within AL (Fig. 2*B*), allowed testing of a hypothesis that NPC dissociation relieved attenuation of IP_3R activity. However, the fact that AL sank beyond resolvable imaging depth during normal maturation precluded imaging analysis of IP_3R functionality during this period of particular interest. Therefore, we investigated the effects of cytoskeletal inhibition on ER remodelling, with the goal of impeding the AL movements that precluded continuous imaging throughout maturation. Incubation of oocytes in nocodazole (70 μM), a microtubule-disrupting agent, had little effect on AL in resting oocytes and cortical ER patch dynamics during oocyte maturation (Fig. 3*Aa*). In contrast, manipulation of actin microfilaments, with cytochalasin or jasplakinolide, markedly altered the dynamics of ER remodelling. Both agents inhibited the sinking and normal fragmentation of AL into smaller patches (phase 2), such that individual AL could now be tracked throughout maturation as they condensed into single, often abnormally large, cortical ER patches (Fig. 3*Ab* and *c*, Supplemental Movie 6). As with nocodazole, neither compound disrupted AL organization in the resting oocyte. Quantitative analyses of cortical ER patch properties revealed that microfilament disruption inhibited ER patch movement (Fig. 3*B*) and increased average patch size (Fig. 3*C*). Notably, the population histogram of patch size displayed rightward shifts in the presence of the actin-modifying agents, with the increased population mean (cytochalasin $12.5 \pm 1.7\ \mu m^2$, jasplakinolide $11.2 \pm 1.5\ \mu m^2$ *versus* control $8.4 \pm 0.3\ \mu m^2$) reflecting the population of 'mega'-patches condensed from individual AL (Fig. 3*C*). Since this manipulation permitted resolution of AL throughout the maturation process, we investigated whether cytoskeletal disruption affected NPC dissociation. Treatment with either cytochalasin (Fig. 3*D*) or jasplakinolide (data not shown) did not impact NPC dissociation judged by the time course or the 'mosaic'

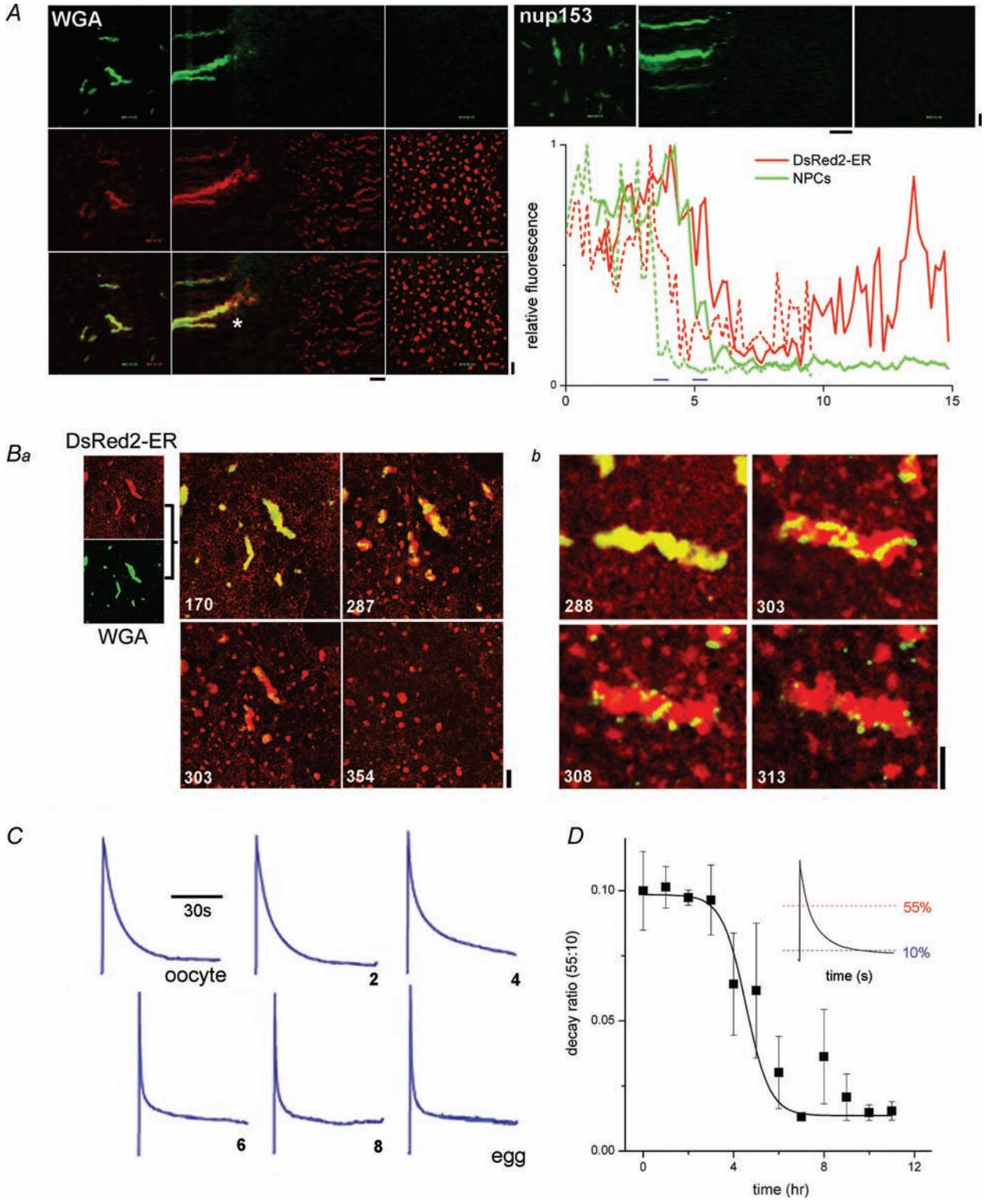

Figure 2. Nucleoporin and macroscopic Ca^{2+} dynamics during oocyte maturation
A, time course of nucleoporin dissociation from AL. Left, composite lamellogram of a maturing cell expressing DsRed2-ER (red), injected with Alexa Fluor 488-WGA (green), with the dual-channel fluorescence overlay shown at bottom. Confocal ('*xy*') images are shown at the start ($t = 1$ h, left) and the end ($t = 15$ h, right) of a timelapse record (Supplemental Movie 3). Right, time course of nup153-GFP dissociation during maturation. Representative fluorescence profiles of ER remodelling (red) and NPC dissociation (green) in cells expressing DsRed2-ER and nup153 (dotted lines) or DsRed2-ER alone and injected with Alexa Fluor 488-WGA (green). Time delays between NPC and

appearance of AL during NPC disassembly. Therefore, we exploited this method to permit imaging of AL Ca^{2+} dynamics during NPC dissociation within the live cell.

First, we looked at numerous AL (at different points during maturation), and correlated the capacity of IP_3Rs within AL to trigger Ca^{2+} waves (Fig. 4*A*, inset) relative to the density of NPCs on individual AL at that time point. As an index of NPC presence, we used the ratio of DsRed2-ER fluorescence intensity (ER label) to WGA fluorescence intensity (NPC label). The ratio (ER : WGA) increased as NPCs dissociated from AL. Considering the population of AL as a whole, this dataset revealed that the higher the intensity of WGA staining, the lower the likelihood of AL IP_3Rs initiating Ca^{2+} waves in response to IP_3 (Fig. 4*Aa*, Supplemental Movie 7). Even in a single cell, at the *same* time point, where AL in different parts of the vegetal hemisphere could be resolved at different stages of NPC disassembly, individual NPC-depleted AL were more active than AL decorated with NPCs (Fig. 4*Ab*).

Second, we collated the activity of IP_3Rs within AL subdomains over different time periods during maturation and compared the time course of relief of IP_3R inhibition with the time course of NPC disassembly. A strong temporal correlation was observed between the abrupt change in NPC integrity (ER : WGA ratio) and the capacity of AL to nucleate Ca^{2+} waves (Fig. 4*B*). In summary, both spatial (Fig. 4*A*) and temporal (Fig. 4*B*) macroscopic datasets indicate that the presence of intact NPCs on AL correlates with decreased local IP_3R activity.

Using video-rate confocal microscopy, Ca^{2+} puffs were mapped at low levels of stimulation and their localization correlated with AL morphology during the period of NPC disassembly. To analyse these triple colour imaging experiments, composite overlays of NPC distribution throughout AL were generated to assess the location of active IP_3R clusters relative to NPC distribution (Fig. 4*C*). Visual inspection of these records demonstrated that Ca^{2+} puffs within AL first appeared in regions free from NPCs (Fig. 4*C*), with NPC-replete regions of the same ER structure remaining devoid of Ca^{2+} puff activity. Such observations were quantified by collating the WGA fluorescence intensity at Ca^{2+} puff sites relative to the range of WGA fluorescence values observed throughout the AL at the same time point (Fig. 4*D*). These data show that sites of Ca^{2+} puff activity occurred within regions of a single AL with low NPC occupancy (Fig. 4*D*), again suggesting that NPC dissociation indirectly/directly facilitated a gain-of-functionality transition in Ca^{2+} signalling competency of IP_3Rs.

What triggers NPC dissociation from AL? Injection of okadaic acid in the absence of progesterone, a protein phosphatase 1 and 2A inhibitor, caused rapid AL disassembly and decreased the duration of phase 1 ('AL persistence') from 4.3 ± 1.5 h to ≤ 1 h (Fig. 5*A*). Consistent with models for regulation of NPC (dis)assembly in the nuclear envelope, these data implicate a kinase/phosphatase cycle controlling AL remodelling (Onischenko *et al.* 2005). A likely candidate kinase is the maturation promoting factor (MPF) kinase (a cyclin B and cdc2/cdk1 heterodimer), given its role in maturation and as an *in vitro* effector of NPC disassembly at nuclear envelope breakdown (NEBD) (Favreau *et al.* 1996; Onischenko *et al.* 2005; Muhlhausser & Kutay, 2007). Indeed, whole-cell kinase assays demonstrated that the time course of MPF activation correlated well with AL remodelling (Fig. 5*B*). Moreover, measurements of MPF activity in single cells performed when NPCs were observed to be dissociating from AL (by live cell imaging) were higher than in cells where AL were static and NPCs were intact (Fig. 5*B*, inset). Finally, okadaic acid caused a rapid increase in MPF activity (Fig. 5*B*), mimicking the accelerated time course of AL disassembly (Fig. 5*A*).

These data imply that MPF activation parallels the timeframe of AL disappearance, and that the kinase is 'globally' active in cells where AL remodelling is occurring, but do not demonstrate that MPF is active in the *local* vicinity of AL prior to NPC dissociation, as expected if this kinase was a key trigger for NPC dissociation *in vivo*. Therefore, to monitor endogenous MPF activity, we expressed a GFP-tagged vimentin, a substrate for MPF that targets the oocyte cortex (Dent *et al.* 1992). Vimentin is phosphorylated by MPF at a site in the NH_2-terminus (Ser-55), the phosphorylation status of which can be resolved using phospho-specific antibodies. Therefore, by monitoring the co-localization of punctate GFP-vimentin fluorescence with phosphorylation-dependent

AL disappearance were estimated at half-maximal relative fluorescence, and indicated by blue bars. Horizontal time bars = 1 h. *Ba*, confocal images of a maturing cell expressing DsRed2-ER (red) and injected with Alexa Fluor 488-WGA (green). Individual fluorescence images are merged as an overlay shown at various times (numbered in minutes) after progesterone addition (Supplemental Movie 4). Image stills show NPC dissociation from AL over ~1 h interval, captured ~5 h after progesterone exposure. *Bb*, higher magnification images of AL morphology during NPC dissociation. *C*, cellular Ca^{2+} signals evoked by photolytic release of saturating concentrations of IP_3 at indicated time points (hours) during maturation. There was no difference in the magnitude of Ca^{2+} signals, IP_3R sensitivity or maturation competence between cells expressing DsRed2-ER and non-expressing controls. *D*, analysis of time course of changes in the macroscopic Ca^{2+} transient during maturation indexed by following changes in the rate of decay of the transient (ratio of time to decay to 55% and 10% of peak, inset). Vertical scale bars = 10 μm.

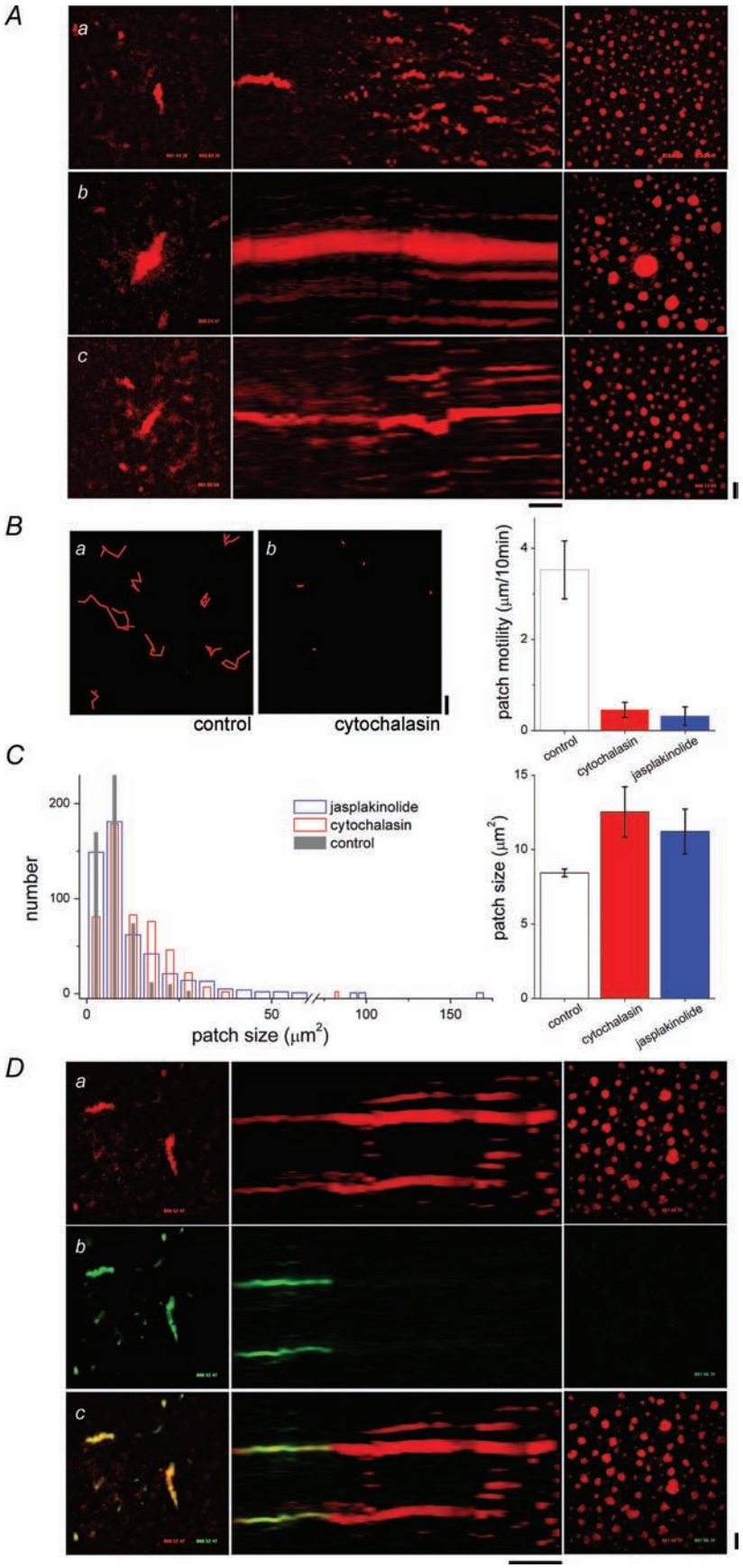

Figure 3. Effect of cytoskeletal disruption on ER remodelling during maturation
A, lamellograms of maturing oocytes subjected to treatment with cytoskeletal-disrupting agents. Sequences show cells treated with 70 μM nocodazole (*a*), 2.5 μM jasplakinolide (*b*, Supplemental Movie 6), and 50 μM cytochalasin B (*c*). Horizontal time bar represents 1 h (*a* and *b*) and 30 min (*c*). *B*, patch motility measured from timelapse records of mature control cells and mature cells treated with cytochalasin or jasplakinolide. Left, tracking patch motility in control (*a*) and cytochalasin-treated cells (*b*) at 10 min intervals from hour-long timelapse records. Right, average patch motility for indicated treatments. *C*, left, histogram showing distribution of patch sizes (cross-sectional area, μm^2) in mature control cells (grey), or cells treated with cytochalasin (red) or jasplakinolide (blue). Right, average patch size for different treatments. *D*, composite lamellogram of a cell expressing DsRed2-ER (*a*) and injected with Alexa Fluor 488-WGA (*b*) matured in the presence of cytochalasin (middle) with the overlay (*c*) shown at bottom. Horizontal time bar represents 1 h. All vertical scale bars = 10 μm.

immunoreactivity, it was possible to identify when, and where, endogenous MPF became active. Figure 5*C* shows the punctate profile and dynamics of vimentin-GFP in the periphery of a live oocyte (Supplemental Movie 8). After immunostaining, little co-localization of GFP fluorescence with phospho-antibody staining was observed in oocytes (Fig. 5*Da*), in contrast to a strong fluorescence overlap observed in eggs (Fig. 5*Db*), as expected if the assay correctly reports MPF activity. Analysis of fluorescence staining in oocytes (fixed at ∼15 min intervals during maturation), at the time point immediately preceding observation of NPC dissociation in live cells, revealed local phosphorylation of vimentin epitope within the vicinity of AL (Fig. 5*D*). Such images suggest that MPF is active locally in the maturing oocyte cortex, immediately prior to AL remodelling.

How does the presence of NPCs regulate local IP_3R activity in AL? Both direct and indirect mechanisms are plausible: direct mechanisms would rely on structural or functional interactions between NPCs and IP_3Rs;

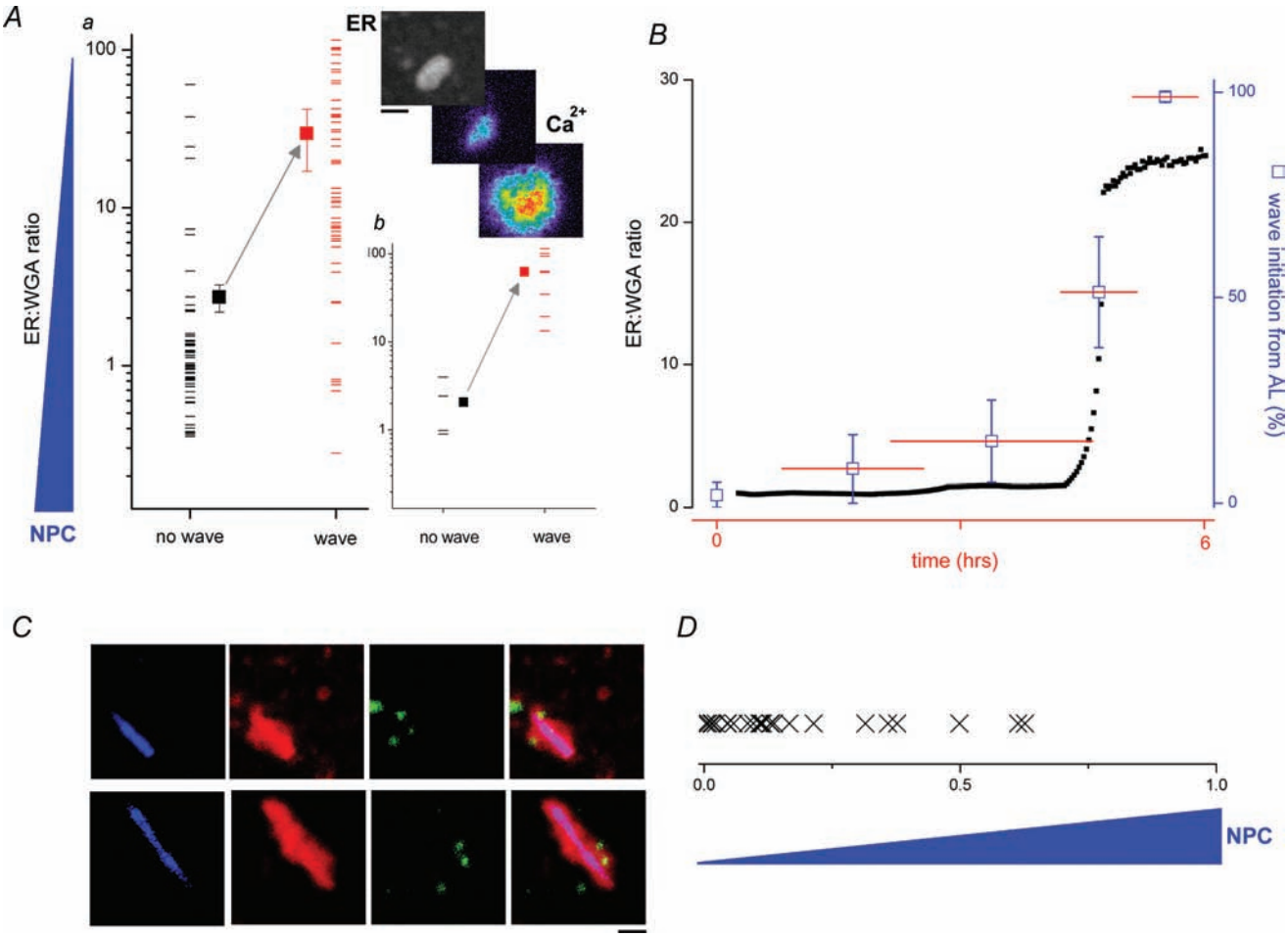

Figure 4. NPC disassembly relieves inhibition of IP_3Rs within AL
Aa, AL population measurement showing correlation between NPC presence on AL (ER : WGA ratio, i.e. value increases with NPC dissociation) and probability of Ca^{2+} wave initiation (black = no wave; red = wave for individual measurements). Filled squares depict population average. *Ab*, single time point data from a single cell, correlating NPC density on different AL (ER : WGA ratio) throughout the ooplasm with Ca^{2+} signalling phenotype. Top, and Supplemental Movie 7, example of WGA-depleted AL (DsRed2-ER, greyscale) initiating a Ca^{2+} wave (pseudocolour) seen at time points ∼500 ms apart. *B*, temporal correlation between ER : WGA ratio (black squares, left ordinate) and Ca^{2+} wave initiation from AL pooled over different time bins after progesterone addition. Horizontal lines (red) represent overlapping time windows (*x*-axis), vertical lines (blue) represent error bars for Ca^{2+} measurements (right ordinate). *C*, representative image stills showing distribution of WGA (blue), DsRed2-ER (red) and Ca^{2+} puffs (green) from two different AL captured during NPC dissociation. Composite three-channel overlay is shown at right. Scale bar = 5 μm *D*, population measurements of Ca^{2+} puff localization on AL during NPC dissociation revealed that the majority of Ca^{2+} puffs localized ('X') to regions of AL showing lower staining with WGA. Horizontal axis represents normalized WGA fluorescence within the AL encompassing the gradient of WGA fluorescence intensities from '0' (lowest WGA) to '1' (maximal WGA intensity).

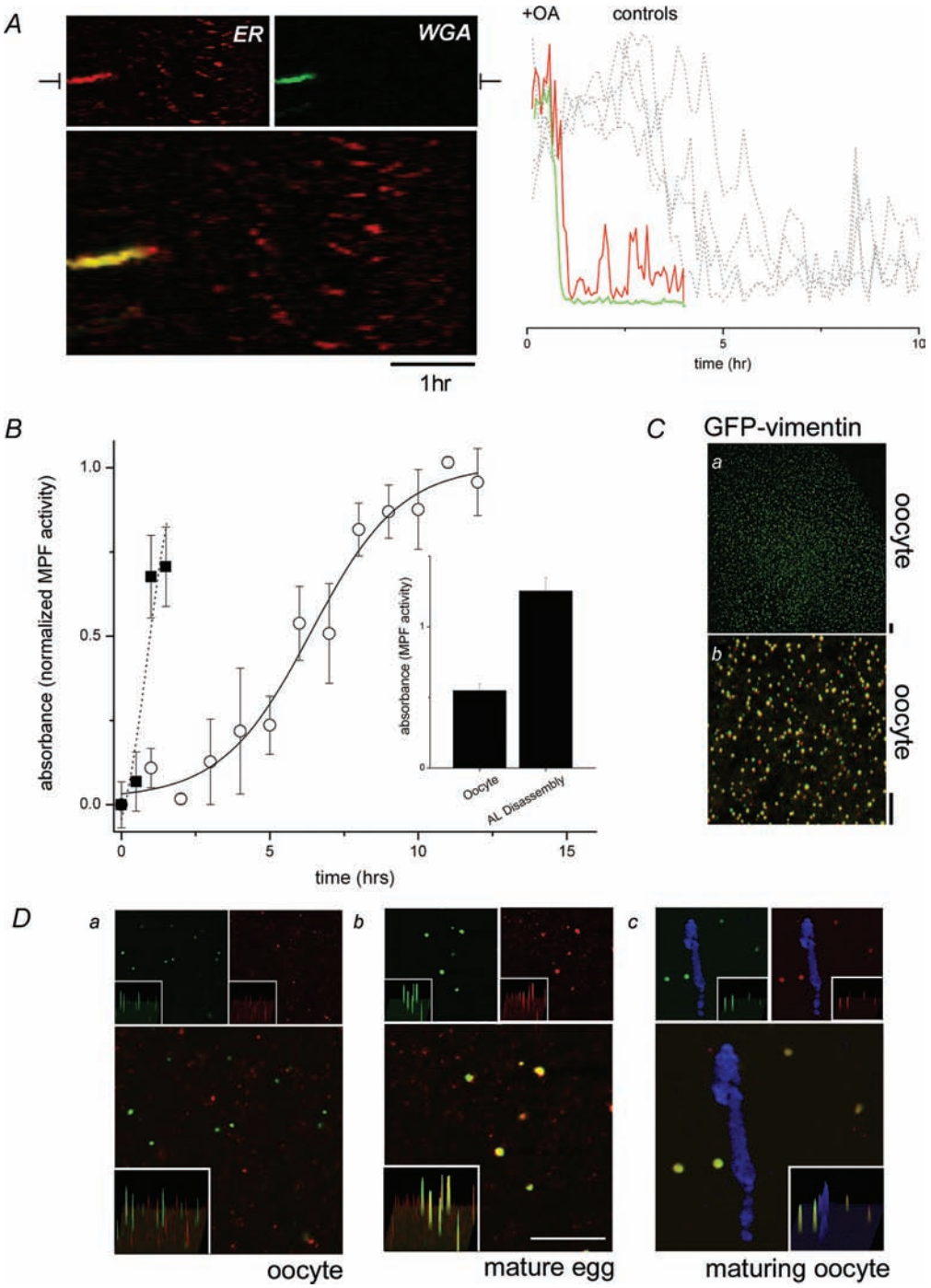

Figure 5. MPF is a candidate kinase for AL disassembly
A, okadaic acid (OA) triggers rapid remodelling of AL. Left, lamellogram showing rapid AL disappearance in an OA-treated cell. Right, associated fluorescence profiles taken from the indicated lamellogram section showing the time course of ER (DsRed2-ER, red) and NPC (WGA, green) disappearance compared with DsRed2-ER profiles from four maturing, parallel controls not exposed to OA (multiple dashed lines). *B*, MPF kinase assay (A_{490}, normalized to levels observed in mature eggs) in maturing oocytes (○) and oocytes treated with OA alone (■). Inset, relative levels of MPF activity (A_{490}) in oocytes and maturing oocytes in which AL were visibly remodelling, assessed by live cell imaging of NPC dissociation. *Ca*, confocal (*xy*) image of an oocyte expressing GFP-vimentin (Supplemental Movie 8). *Cb*, fluorescence overlay of confocal images taken at $t = 0$ (red) and $t = 2$ s (green) highlight considerable motility of some of the GFP-vimentin puncta. Scale bars = 10 μm. *D*, immunofluorescence staining of phospho-vimentin (red, top right), compared with GFP-vimentin (green, top left) by dual colour overlay (bottom) in both lateral ('xy') and 3-D projection (insets). Representative images are shown from an oocyte (*a*), an egg (*b*) and from the vicinity of an AL (WGA, blue) in a maturing cell (*c*). Scale bar = 10 μm.

indirect regulation would depend upon the architectural effects of ER membranes themselves (e.g. membrane curvature; Botelho *et al.* 2006), effects of IP_3R clustering on IP_3R function, or (in)accessibility of sensitizing/inhibitory regulators. Distinguishing these possibilities in the context of AL organization in the intact cell is not straightforward. Two pieces of experimental evidence, however, lend weight to indirect architectural regulation of IP_3Rs within AL.

First, there is no fundamental difference in IP_3R sensitivity between ER- and AL-resident IP_3Rs when intact cell architecture is disrupted by homogenization. To test IP_3R functionality within AL, we optimized a homogenization and fractionation protocol to isolate AL-derived membrane vesicles (marked by enrichment of the nucleoporin p62) using discontinuous sucrose gradient fractionation (Meier *et al.* 1995). In oocytes, an AL-derived vesicle population, shown by immunoblotting to be enriched in p62 and IP_3Rs was isolated in the 'heavy' (56%) fraction (Fig. 6*A*). Notably, the immunoreactivity of this fraction decreased in eggs (Fig. 6*A*), consistent with the observed disassembly of AL during meiotic maturation (Boulware & Marchant, 2005). In parallel, IP_3R immunoreactivity was transferred into the lighter (43%), cortical ER fraction recapitulating the IP_3R redistribution from AL into cortical ER patches observed in live cells (Fig. 3). IP_3 responsiveness of the relevant vesicle populations was determined in $^{45}Ca^{2+}$ efflux assays (Fig. 6*B*). As expected, the light (43%) cortical ER fractions derived from whole eggs and oocytes both released Ca^{2+} in response to IP_3 (EC_{50} 32 ± 2 nM and 47 ± 13 nM, respectively, $n = 3$) with a larger observed store size in eggs than oocytes ($38.9 \pm 3.4\%$ and $28.5 \pm 8.0\%$, $n = 6$). Noticeably, the AL fraction from oocytes (56%) also released Ca^{2+} in response to IP_3 over a similar concentration range (EC_{50} of 41 ± 6 nM) to that seen in cortical ER fractions. These results suggest that there is no fundamental difference in IP_3 sensitivity between these ER fractions that is bridged, for example, by a gain-of-function phosphorylation or loss of an inhibitory factor during maturation. AL in oocytes do contain IP_3Rs capable of activation and their activity is more likely attenuated by architectural considerations within intact AL that are disrupted by homogenization, or physiologically reorganized during maturation by MPF-triggered disassembly of NPCs (Figs 2, 4, 5 and 6). No Ca^{2+} release was observed from the AL (56%) fraction in eggs ($n = 1$) indicating that the Ca^{2+} release in the oocyte fraction was not an artifact of contaminating ER (Fig. 6*B*).

Second, a significant architectural reorganization of ER membranes ensues after NPC dissociation, as evidenced by a permeability transition to high molecular weight dextrans previously excluded from AL. AL membranes in oocytes did not pose a barrier to ~10 kDa dextran conjugates. However, several types of 70 kDa fluorescently tagged dextran molecules were initially excluded from AL when injected alone into oocytes. During maturation, the permeability of AL to 70 kDa dextrans increased (Fig. 6*C*, Supplemental Fig. 2) consistent with a morphological reorganization associated with NPC dissociation. Therefore, both the $^{45}Ca^{2+}$ flux and morphological data support the general concept of indirect attenuation of IP_3R activity, relieved by nucleoporin disassembly.

Discussion

Understanding ER heterogeneity is important: the overall functionality of an organelle integrates the properties and prevalence of the subdomains existing within a cell at any given time. In *Xenopus* oocytes, the vast majority of NPCs ($> 80\%$) are not found as would be expected within the nuclear envelope, but in understudied specializations of the rough ER known as annulate lamellae (Cordes *et al.* 1995). Here, we discuss three issues relevant to AL: What is their cellular role? How do they assemble and disassemble? How is IP_3R activity locally attenuated within AL?

A new role for annulate lamellae

Over the years, a variety of roles have been ascribed to AL (Kessel, 1992) with the prevalent consensus being that AL are stockpiles of excess nucleoporins to support subsequent, rapid cell divisions. However, careful quantification of AL number and nucleoporin localization during proliferation in early *Drosophila* embryos challenged this idea (Onischenko *et al.* 2004). Our data also suggest a wider role for AL beyond solely nucleoporin 'warehousing' that stresses the functional consequences of ER protein residency within these subdomains. We propose that targeting of ER proteins into AL may attenuate their functionality, suppressing their involvement in cellular events up to the point when AL are remodelled and AL-resident proteins rejoin the bulk ER/cytosol (Fig. 7). Therefore, the genesis of AL provides a cell with a chronic mechanism ($\geq$ hours) for regulating ER protein activity, by localizing proteins within these discrete ER subdomains where their activity is suppressed. Scenarios of AL biogenesis would then encompass preparative, physiological adaptations to support rapid, 'gain-of-function' transitions in cellular behaviour on AL remodelling, but also as a way of minimizing the impact of proteins that may impair ER functionality. In this context, it is noteworthy that several studies report increased numbers of AL ($\leq$ 3-fold) in virally infected cells, consistent with targeting of viral glycoproteins into these ER subdomains (Kessel, 1992; Cardinali *et al.* 1998).

If this idea is correct, what is the physiological rationale for compartmentalization of proteins shown to localize to AL (IP_3Rs, NPCs, cyclin-B2 and viral glycoproteins)? For IP_3Rs, the transient, gain-of-function of IP_3Rs

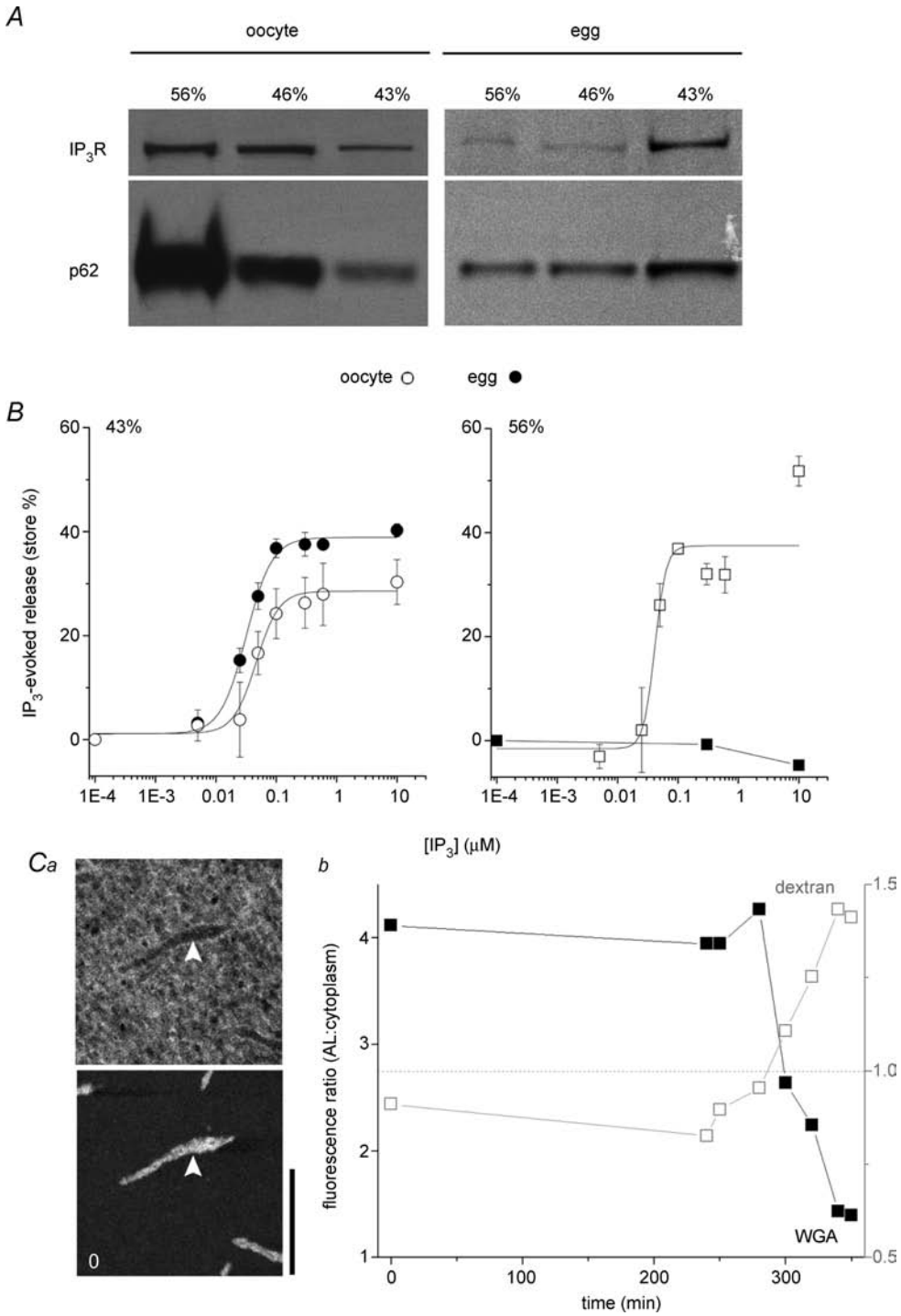

Figure 6. Structural inhibition of IP_3Rs in AL
A, immature oocytes were homogenized and fractionated through a discontinuous sucrose gradient to yield 'heavy' vesicles derived from AL (56%), a population of cortical ER vesicles (43%) and an intermediate mixed vesicular population (46%). The same protocol was utilized on naturally shed eggs. Equal amounts of protein from each fraction were subjected to immunoblotting with anti-IP_3R or anti-p62 antibodies. *B*, left, IP_3 evoked $^{45}Ca^{2+}$ release from the light membrane fraction (43%) extracted from oocytes (○) or eggs (●). Right, IP_3 evoked $^{45}Ca^{2+}$ release from the heaviest membrane fraction (AL) extracted from oocytes (○) or eggs (●). *C*, altered membrane architecture of AL following NPC dissociation: *a*, image stills showing distribution of a 70 kDa fluorescent dextran (top) and a fluorescently tagged WGA conjugate (bottom) with respect to the same AL (white arrows) before maturation ($t = 0$ min, scale bar = 20 μm); *b*, ratio of fluorescence of WGA (■, left ordinate) and dextran fluorescence (□, right ordinate) labelling of AL relative to randomly chosen surrounding cytoplasmic area at the indicated time points during maturation (minutes). Values below dashed grey line (ratio = 1, right ordinate) indicates exclusion from AL.

released from AL in the vegetal hemisphere during oocyte maturation probably facilitates propagation of the fertilization Ca^{2+} wave (Boulware & Marchant, 2005). For NPCs, although presence in AL is futile in terms of transport (mediating cytoplasmic-to-cytoplasmic transfer), NPCs are the keystones that coordinate AL formation. Further, NPC compartmentalization provides a rapidly mobilizable pool of NPCs to impact nucleocytoplasmic transport and gene expression when integrated back into the nuclear envelope. Future studies of NPC density, a parameter that varies with cellular metabolic activity (Hetzer *et al.* 2005), to address whether increases in NPC density can facilitate gene transcription and mRNA export during transcriptional activation of the zygotic genome are warranted. Similarly, correlation between changes in nucleocytoplasmic transport observed in transformed, cancerous cells (Poon & Jans, 2005) and increases in NPC compartmentalization within AL merits investigation. Finally, the targeting of cyclin-B2 (as a pre-MPF component) to AL (Beckhelling *et al.* 2003) probably facilitates localized activation and release of a bolus of MPF when cued (Beckhelling *et al.* 2003), but may also prevent inappropriate activation of cdc2 by segregation of pre-MPF into an ER domain where Ca^{2+} signalling is attenuated.

Mechanisms of AL (dis)assembly

The NPC is a large, complex structure. More than 100 proteins must be recruited from the cytoplasm (multiple copies of individual nucleoporins) to assemble a single NPC. At 125 MDa, it occupies a considerably larger volume than AL-contained ribosomes or IP_3Rs (~35-fold and ~110-fold smaller volumes, respectively). There are few consistently reported differences in NPC composition between NE and AL (Cordes *et al.* 1997; Miller & Forbes, 2000), although AL lack nuclear lamina, matrix and chromatin-associated proteins. Structurally, AL comprise an interconnected stack of ER membranes, with individual cisternae separated by ~100 nm (Cordes *et al.* 1995). Ultrastructural analyses resolve that the intercisternal gap is bridged by NPCs, implying that AL formation is mediated by NPC interactions (Kessel, 1992; Meier *et al.* 1995). Our *in vivo* imaging data showing that NPC presence is essential for AL integrity supports this model (Fig. 2). Consequently, the structural organization of AL by NPCs imparts a regulable cycle for AL (dis)assembly (Fig. 7), contrasting with the variety of organized smooth ER structures formed by low-affinity interactions between abundant, or overexpressed, ER proteins (Snapp *et al.* 2003), which lack a unifying mechanism to rapidly reverse their formation.

While reversible phosphorylation of a subset of NPC components has long been implicated in the mitotic disassembly of nuclear envelope NPCs, the identity of the relevant *in vivo* kinases (cdk1, casein kinase, PKA and GSK3α all phosphorylate specific nucleoporins *in vitro*), as well as the sites phosphorylated by particular kinases, is surprisingly sparse. Strong *in vivo* evidence for a cdk1/phosphatase cycle in regulating AL NPC (dis)assembly derives from an elegant study showing that NPC assembly/localization depends on cdk1 activity, altered experimentally by temperature shifts using a conditional $cdk1^{ts}$ *Drosophila* mutant (Onischenko *et al.* 2005). These data are consistent with our demonstration of localized MPF activity in the subcortex of maturing cells when and where AL are remodelling (Fig. 5), the inhibitory action of local elevations of Ca^{2+} on the initiation of AL remodelling (data not shown), together with the rapid inhibition of AL perdurance after okadaic acid injection (Fig. 5).

Finally, in addition to NPC phosphorylation, cytoskeletal-dependent 'shearing' events facilitate NEBD. In mammalian somatic cells, evidence supports a role for microtubules and microtubule-associated motors (Beaudouin *et al.* 2002; Salina *et al.* 2002). In contrast,

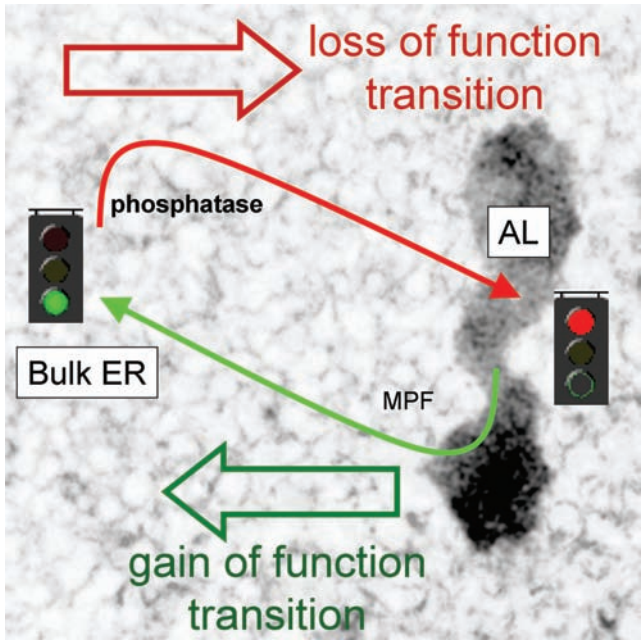

Figure 7. Proposed role for AL in regulating ER protein activity
Hypothesized role for AL assembly/disassembly in regulating the activity of ER resident proteins. ER proteins resident within AL (right) display attenuated function compared to their properties when resident within the bulk ER (left). Therefore regulated assembly/disassembly of AL, effected via a kinase (probably MPF)/phosphatase cycle, is associated with a loss (red)/gain (green) of function transition in protein activity. Regulated AL disassembly provides a mechanism for physiological 'gain-of-function' transitions, and pathologically AL assembly is probably an adaptation to sequester proteins when exogenous protein overload (e.g. viral infection) may impair ER functionality.

our data implicate microfilament-critical steps in AL remodelling (Fig. 3; Muhlhausser & Kutay, 2007). Microfilament disruption inhibited the morphological rearrangements that accompany both AL sinking and AL disaggregation into smaller, cortical ER densities. Whether this difference reflects specialized roles for microtubules and microfilaments in NEBD and AL remodelling, or simply differences in the role of cytoskeletal filaments between mammalian and non-mammalian systems remains to be established.

IP_3R functionality within AL

We believe decreased IP_3R activity within AL is most likely an indirect consequence of the architectural role of NPCs in forming this ER subdomain, rather than any direct effects of NPCs on IP_3R. A speculative mechanism may relate to changes in optimal IP_3R architecture enforced by spatial constraints on IP_3R clustering resulting from the high density of NPCs and IP_3Rs within intact AL (40–70 NPCs μm^{-2} in AL; Cordes *et al.* 1995; Hoppener *et al.* 2005). The elementary, functional unit of IP_3-dependent local Ca^{2+} signalling in intact cells is the 'Ca^{2+} puff' (Parker *et al.* 1996; Bootman *et al.* 1997), an activity-dependent measure of Ca^{2+} channel recruitment within an IP_3R 'cluster'. In the absence of structural data, the underlying IP_3R architecture is inferred from confocal linescan images of Ca^{2+} release profiles, interpreted as being consistent with coordinated opening of ∼30 (25–35) IP_3Rs within a region ∼550 nm (300–800 nm) wide (Shuai *et al.* 2006). Therefore, the optimal IP_3R 'cluster' producing Ca^{2+} puffs in the bulk ER appears (at least from *functional* measurements) to be a loosely corralled unit (mean separation between active IP_3Rs of ∼80 nm, a distance ∼4-fold greater than the lateral dimension of a tetrameric IP_3R; Taylor *et al.* 2004). Modelling predictions that support the 'diffuse' organization of active IP_3Rs within Ca^{2+} puffs (Shuai *et al.* 2006) are consistent with microscopic Ca^{2+} release patterns *within* individual Ca^{2+} puff sites (Bootman *et al.* 1997; Demuro & Parker, 2008). If such an organization of IP_3Rs is a prerequisite for observation of local IP_3R activity, then attenuated responsiveness of IP_3Rs in AL may simply result from an inability to adopt this favoured distribution. Higher IP_3R density, and increased IP_3R proximity enforced by NPC packing (free space between NPCs of only ∼50 nm in AL) may preclude organization of IP_3Rs into architectures optimal for local Ca^{2+} signalling – perhaps via modulation of local Ca^{2+} feedback effects (Means *et al.* 2006) or direct conformational uncoupling – until NPC disassembly has occurred (Fig. 4). Consistent with this theme, others have speculated that the high density packing of IP_3Rs observed in cerebellar Purkinje cells inhibits IP_3R function (Satoh *et al.* 1990; Katayama *et al.* 1996). Smooth ER cisternal stacks/vesicles (containing IP_3Rs at ∼10-fold the density of adjacent rER, Satoh *et al.* 1990; or as arrays of IP_3Rs where individual channels physically contact each other, Katayama *et al.* 1996) increase rapidly in hypoxic scenarios, possibly as an adaptation to decrease ER Ca^{2+} efflux (Satoh *et al.* 1990; Takei *et al.* 1994; Katayama *et al.* 1996). Such a pool of high density, attenuated IP_3Rs is consistent with the low IP_3 sensitivity of intact Purkinje neurons (tens of micromolar; Khodakhah & Ogden, 1993). Similarly, higher-order IP_3R 'aggregations' (those visible by fluorescence microscopy) seen in the ER after maintained IP_3R stimulation, are associated with suppression of whole-cell Ca^{2+} signals (Wilson *et al.* 1998; Tateishi *et al.* 2005; Chalmers *et al.* 2006; Means *et al.* 2006). None-the-less, further studies of AL organization and composition would be needed to better understand the regulatory environment of IP_3Rs in AL. Although the morphological continuity between the ER membranes often leads to the assumption of equivalency, the composition of different ER regions is divergent, a finding underscored by large-scale, subtractive proteomics (Schirmer *et al.* 2003).

We conclude that relief of IP_3R inhibition is correlated with the physiological dismantling of NPCs from the same, local regions of ER. Physiological disassembly of NPCs during oocyte maturation, effected via targeted phosphorylation of nucleoporins by maturation kinases, notably MPF, yields NPC-denuded ER domains that we show via multicolour imaging experiments correlate spatially and temporally with increased IP_3R activity.

References

Baumann O & Walz B (2001). Endoplasmic reticulum of animal cells and its organization into structural and functional domains. *Int Rev Cytol* **205**, 149–214.

Beaudouin J, Gerlich D, Daigle N, Eils R & Ellenberg J (2002). Nuclear envelope breakdown proceeds by microtubule-induced tearing of the lamina. *Cell* **108**, 83–96.

Beckhelling C, Chang P, Chevalier S, Ford C & Houliston E (2003). Pre-M phase-promoting factor associates with annulate lamellae in *Xenopus* oocytes and egg extracts. *Mol Biol Cell* **14**, 1125–1137.

Blaustein MP & Golovina VA (2001). Structural complexity and functional diversity of endoplasmic reticulum Ca^{2+} stores. *Trends Neurosci* **24**, 602–608.

Bootman MD, Niggli E, Berridge MJ & Lipp P (1997). Imaging the hierarchical Ca^{2+} signalling system in HeLa cells. *J Physiol* **499**, 307–314.

Borgese N, Francolini M & Snapp E (2006). Endoplasmic reticulum architecture: structures in flux. *Curr Opin Cell Biol* **18**, 358–364.

Botelho AV, Huber T, Sakmar TP & Brown MF (2006). Curvature and hydrophobic forces drive oligomerization and modulate activity of rhodopsin in membranes. *Biophys J* **91**, 4464–4477.

Boulware MJ & Marchant JS (2005). IP_3 receptor activity is differentially regulated in endoplasmic reticulum subdomains during oocyte maturation. *Curr Biol* **15**, 765–770.

Callamaras N & Parker I (1999). Construction of a confocal microscope for real-time x-y and x-z imaging. *Cell Calcium* **26**, 271–279.

Cardinali G, Gentile M, Cirone M, Zompetta C, Frati L, Faggioni A & Torrisi MR (1998). Viral glycoproteins accumulate in newly formed annulate lamellae following infection of lymphoid cells by human herpes virus 6. *J Virol* **72**, 9738–3976.

Chalmers P, Schell MJ & Thorn P (2006). Agonist-evoked inositol trisphosphate receptor (IP_3R) clustering is not dependent on changes in the structure of the endoplasmic reticulum. *Biochem J* **394**, 57–66.

Cordes VC, Reidenbach S & Franke WW (1995). High content of a nuclear pore complex protein in cytoplasmic annulate lamellae of *Xenopus* oocytes. *Eur J Cell Biol* **68**, 240–255.

Cordes VC, Reidenbach S, Rackwitz HR & Franke WW (1997). Identification of protein p270/Tpr as a constitutive component of the nuclear pore complex-attached intranuclear filaments. *J Cell Biol* **136**, 515–529.

Demuro A & Parker I (2008). Multi-dimensional resolution of elementary Ca^{2+} signals by simultaneous multi-focal imaging. *Cell Calcium* 43, 367–374.

Dent JA, Cary RB, Bachant JB, Domingo A & Klymkowsky MW (1992). Host cell factors controlling vimentin organization in the *Xenopus* oocyte. *J Cell Biol* **119**, 855–866.

El-Jouni W, Jang B, Haun S & Machaca K (2005). Calcium signaling differentiation during *Xenopus* oocyte maturation. *Dev Biol* **288**, 514–525.

Favreau C, Worman HJ, Wozniak RW, Frappier T & Courvalin JC (1996). Cell cycle-dependent phosphorylation of nucleoporins and nuclear pore membrane protein Gp210. *Biochemistry* **35**, 8035–8044.

Finlay DR, Newmeyer DD, Price TM & Forbes DJ (1987). Inhibition of in vitro nuclear transport by a lectin that binds to nuclear pores. *J Cell Biol* **104**, 189–200.

Golovina VA & Blaustein MP (1997). Spatially and functionally distinct Ca^{2+} stores in sarcoplasmic and endoplasmic reticulum. *Science* **275**, 1643–1648.

Hetzer MW, Walther TC & Mattaj IW (2005). Pushing the envelope: structure, function and dynamics of the nuclear periphery. *Ann Rev Cell Dev Biol* **21**, 347–380.

Hoppener C, Siebrasse JP, Peters R, Kubitscheck U & Naber A (2005). High-resolution near-field optical imaging of single nuclear pore complexes under physiological conditions. *Biophys J* **88**, 3681–3688.

Katayama E, Funahashi H, Michikawa T, Shiraishi T, Ikemoto T, Iino M, Hirosawa K & Mikoshiba K (1996). Native structure and arrangement of inositol-1,4,5-trisphosphate receptor molecules in bovine cerebellar Purkinje cells as studied by quick-freeze deep-etch electron microscopy. *EMBO J* **15**, 4844–4851.

Kessel RG (1992). Annulate lamellae: a last frontier in cellular organelles. *Int Rev Cytol* **133**, 43–120.

Khodakhah K & Ogden D (1993). Functional heterogeneity of calcium release by inositol trisphosphate in single Purkinje neurones, cultured cerebellar astrocytes, and peripheral tissues. *Proc Natl Acad Sci U S A* **90**, 4976–4980.

Lievremont J-P, Hill A-M, Hilly M & Mauger J-P (1994). The inositol 1,4,5-trisphosphate receptor is localized on specialized sub-regions of the endoplasmic reticulum in rat liver. *Biochem J* **300**, 419–427.

Liou J, Kim LM, Heo WD, Jones JT, Myers JW, Ferrell JE Jr & Meyer T (2005). STIM is a Ca^{2+} sensor essential for Ca^{2+} store depletion triggered Ca^{2+} influx. *Curr Biol* **15**, 1235–1241.

Means S, Smith AJ, Shepherd J, Shadid J, Fowler J, Wojcikiewicz RJH, Mazel T, Smith GD & Wilson BS (2006). Reaction diffusion modeling of calcium dynamics with realistic ER geometry. *Biophys J* **91**, 537–557.

Meier E, Miller BR & Forbes DJ (1995). Nuclear pore complex assembly studied with a biochemical assay for annulate lamellae formation. *J Cell Biol* **129**, 1459–1472.

Meldolesi J & Pozzan T (1998). The heterogeneity of ER Ca^{2+} stores has a key role in non-muscle cell signaling and function. *J Cell Biol* **142**, 1395–1398.

Miller BR & Forbes DJ (2000). Purification of the vertebrate nuclear pore complex by biochemical criteria. *Traffic* **1**, 941–951.

Miller BR, Powers M, Park M, Fischer W & Forbes DJ (2000). Identification of a new vertebrate nucleoporin, Nup188, with the use of a novel organelle trap assay. *Mol Biol Cell* **11**, 3381–3396.

Mogami H, Nakano K, Tepikin AV & Petersen OH (1997). Ca^{2+} flow via tunnels in polarized cells: recharging of apical Ca^{2+} stores by focal Ca^{2+} entry through basal membrane patch. *Cell* **88**, 49–55.

Muhlhausser P & Kutay U (2007). An in vitro nuclear disassembly system reveals a role for the RanGTPase system and microtubule-dependent steps in nuclear envelope breakdown. *J Cell Biol* **178**, 595–610.

Onischenko EA, Gubanova NV, Kieselbach T, Kiseleva EV & Hallberg E (2004). Annulate lamellae play only a minor role in the storage of excess nucleoporins in *Drosophila* embryos. *Traffic* **5**, 152–164.

Onischenko EA, Gubanova NV, Kiseleva EV & Hallberg E (2005). Cdk1 and okadaic acid-sensitive phosphatases control assembly of nuclear pore complexes in *Drosophila* embryos. *Mol Biol Cell* **11**, 5152–5162.

Papp S, Dziak E, Michalak M & Opas M (2003). Is all of the endoplasmic reticulum created equal? The effects of the heterogeneous distribution of endoplasmic reticulum Ca^{2+}-handling proteins. *J Cell Biol* **160**, 475–479.

Parker I, Choi J & Yao Y (1996). Elementary events of $InsP_3$-induced Ca^{2+} liberation in *Xenopus* oocytes: hot spots, puffs and blips. *Cell Calcium* **20**, 105–121.

Poon IKH & Jans DA (2005). Regulation of nuclear transport: central role in development and transformation. *Traffic* **6**, 173–186.

Rooney A & Meldolesi J (1996). The endoplasmic reticulum in PC12 cells. *J Biol Chem* **271**, 29304–29311.

Roos J, DiGregorio PJ, Yeromin AV, Ohlsen K, Lioudyno M, Zhang S, Safrina O, Kozak JA, Wagner SL, Cahalan MD, Velicelebi G & Stauderman KA (2005). STIM1, an essential and conserved component of store-operated Ca^{2+} channel function. *J Cell Biol* **169**, 435–445.

Salina D, Bodoor K, Eckley DM, Schroer TA, Rattner JB & Burke B (2002). Cytoplasmic dynein as a facilitator of nuclear envelope breakdown. *Cell* **108**, 97–107.

Satoh T, Ross CA, Villa A, Supattapone S, Pozzan T, Snyder SH & Meldolesi J (1990). The inositol 1,4,5-trisphosphate receptor in cerebellar Purkinje cells: quantitative immunogold reveals concentration in an ER subcompartment. *J Cell Biol* **111**, 615–624.

Schirmer EC, Florens L, Guan T, Yates JR III & Gerace L (2003). Nuclear membrane proteins with potential disease links found by subtractive proteomics. *Science* **301**, 1380–1382.

Shuai J, Rose HJ & Parker I (2006). The number and spatial distribution of IP_3 receptors underlying calcium puffs in *Xenopus* oocytes. *Biophys J* **91**, 4033–4044.

Snapp EL, Hegde RS, Francolini M, Lombardo F, Colombo S, Pedrazzini E, Borgese N & Lippincott-Schwartz J (2003). Formation of stacked ER cisternae by low affinity protein interactions. *J Cell Biol* **163**, 257–269.

Stoffler D, Fahrenkrog B & Aebi U (1999). The nuclear pro complex: from molecular architecture to functional dynamics. *Curr Opin Cell Biol* **11**, 391–401.

Sutovsky P, Simerly C, Hewitson L & Schatten G (1998). Assembly of nuclear pore complexes and annulate lamellae promotes normal pronuclear development in fertilized mammalian oocytes. *J Cell Sci* **111**, 2841–2854.

Takei K, Mignery GA, Mugnaini E, Südhof TC & De Camilli P (1994). Inositol 1,4,5-trisphosphate receptor causes formation of ER cisternal stacks in transfected fibroblasts and in cerebellar Purkinje cells. *Neuron* **12**, 327–342.

Tateishi Y, Hattori M, Nakayama T, Iwai M, Bannai H, Nakamura T, Michikawa T, Inoue T & Mikoshiba K (2005). Cluster formation of inositol 1,4,5-trisphosphate receptor requires its transition to open state. *J Biol Chem* **280**, 6816–6822.

Taylor CW, Da Fonseca PCA & Morris EP (2004). IP_3 receptors: the search for structure. *Trends Biochem Sci* **29**, 210–219.

Terasaki M & Jaffe LA (1991). Organization of the sea urchin egg endoplasmic reticulum and its reorganization at fertilization. *J Cell Biol* **114**, 929–940.

Voeltz GK, Rolls MM & Rapoport TA (2002). Structural organization of the endoplasmic reticulum. *EMBO Rep* **3**, 944–950.

Wilson BS, Pfeiffer JR, Smith AJ, Oliver JM, Oberdorf JA & Wojcikiewicz RJH (1998). Calcium-dependent clustering of inositol 1,4,5-trisphosphate receptors. *Mol Biol Cell* **9**, 1465–1478.

Acknowledgements

This work was supported by NIH (to J.S.M., grant no. NS046783) and a NSF CAREER Fellowship (to J.S.M., grant no. 0237946).

Supplemental material

Online supplemental material for this paper can be accessed at:
http://jp.physoc.org/cgi/content/full/jphysiol.2008.153379/DC1
and
http://www.blackwell-synergy.com/doi/suppl/10.1113/jphysiol.2008.153379